Modelling and Simulations of a clinical PET-system using the GATE Monte Carlo software

Philip Kalaitzidis

Supervisors

Michael Ljungberg, David Minarik and Cecilia Hindorf

Abstract

Introduction: The increased importance of PET imaging in the health care system has lead to a constant need for improvement and optimisation of scanner systems and their protocols. By utilising the features of the GATE Monte Carlo program one can gain a better understanding of the limitations and possibilities of the system. GATE together with the reconstruction software CASToR provides a link from simulation of modeled system to reconstructed images. The aim of this thesis was to learn the basics of the Monte Carlo method and how to operate GATE, to create a model of a generic PET camera as a first approximation, perform simulations using 18F as radioactive source and from simulated data reconstruct images using the CASToR software.

Material and method: The modelling of the generic camera used the G.E. PET/CT Discovery-690 as a template. The NEMA 2012/IEC 2008 PET phantom was used to perform a measurement on a G.E. PET/CT Discovery-690. CT-images from the measurement were segmented and used as a phantom for simulations. Parameters such as true-fraction, scatter-fraction, random-fraction, sensitivity and FWHM of three spheres were compared between the measurement and the simulation. Simulations of a human-like phantom (XCAT) were also performed and compared to images of clinical exams with 18F-fluoride taken with a Philips Gemini TF PET/CT. Comparisons were also made with a SIMIND SPECT simulation of the same phantom in order to study qualitative differences between PET and SPECT.

Results: The general structure of the simulated image corresponds well with structures in the images taken by the Philips PET/CT Gemini TF camera. The visual comparison between GATE and SIMIND simulated images show similar geometrical structures. True-fraction, scatter-fraction, random-fraction, sensitivity and FWHM between the measurement, NEMA simulation 1 (energy window threshold 300 keV, crystal energy resolution 20%) and NEMA simulations 2 (energy window threshold 425 keV, crystal energy resolution 8%) (M/S1/S2) were TF: 0.64/0.29/0.47, SF: 0.23/0.45/0.32, RF: 0.14/0.27/0.22, S: 5.1/8.3/4.0 cps/kBq, FWHM for three of the sphere 36.0/36.4/35.9 mm, 27.5/25.4/24.2 mm and 16.0/14.5/14.7 mm. NEMA simulation 1 showed high values of scatter- and random-fraction and a large deviation in sensitivity with 63% higher compared to the measurement. After increasing the energy window threshold to 425 keV and crystal energy resolution to 8% (NEMA simulation 2) the results from the measurements and simulations became more in accordance with each other, but are still deviating.

Conclusion: GATE is a powerful tool simulating emission tomography. With the modelling tools provided by the Geant4 kernel, GATE offers the user good possibilities to model specific scanner geometry and set-up. While GATE provides good simulating accuracy it comes at a cost of computational power and time - the need for decreasing simulation time is thus necessary. The link between CASToR and GATE creates a good chain from simulated data to reconstructed images. PET images show better spatial resolution over SPECT images of identical distribution. The results are satisfying with regards to visual properties, however, the quantifiable parameters have a significant deviation that needs to be further investigated as to why the deviations occur. By further improving the model GATE simulations could possibly act as an option in patient studies in the future.

Kan verkligheten verkligen simuleras?

Populärvetenskaplig beskrivning

I verksamheten för diagnostisk medicin är de bildgivande systemens funktion ett ständigt område för förbättring. En metod för utveckling och förbättring av systemen är genom simuleringar. I detta arbete har programmet GATE använts för att modellera och simulera ett PET-system. Simuleringarna har sedan gjorts om till bilder med programmet CASToR för att jämföra resultaten med verkliga undersökningar och mätningar.

PET (Positron emissions tomografi) är en teknik som faller inom området för nuklearmedicin. PET syftar till att studera hur kroppens celler fungerar, och är ett kraftfullt verktyg för diagnostik av bland annat cancer. Med PET innebär att ett radioaktivt ämne injiceras i en patient varpå det ämnet kommer fördela sig i kroppen utefter funktionalitet. Områden som fungerar abnormalt kommer antingen ta upp mer eller mindre av det radioaktiva ämnet. Det radioaktiva ämnet kommer under undersökningen att sönderfalla, vilket resulterar i fotonstrålning som kommer detekteras av PET-kameran. Informationen kan sedan användas för att återskapa bilder och på så vis kan den medicinskt kunniga avgöra huruvida patienten är frisk eller sjuk.

Ett sätt att arbeta med förbättringar inom PET-verksamheten är genom att simulera undersökningar och mätningar. Monte Carlo metoden är ett sådant verktyg som baserat på slumpmässigt genererade tal och genom kända sannolikheter för att en händelse skall ske försöker förutse hur en sekvens av händelser hade sett ut om de hade skett i verklighet. Med en tillräckligt kraftfull dator kan man simulera partikelstrålningen associerad med PET-diagnostik, och på så sätt arbeta med att ständigt förbättra tekniken och undersökningsprotokoll.

För att en simulering skall vara tillräckligt träffsäker i sina resultat måste beskrivningen av simuleringen efterlikna verkligheten. Att således beskriva den simulerade världen korrekt är av yttersta vikt. I fallet för en simulering av en PET-undersökning handlar det då bland annat om kamerans uppbyggnad, korrekt beskriven fysik och detektorns svar på en träff.

GATE är ett simuleringsprogram anpassad inom området för nuklearmedicin, detta program ger användare friheten att skapa sin egen simuleringsgeometri och sedan studera hur partiklar transporteras från start- till slutpunkt. Den insamlade information från simuleringen kan användas för att studera underliggande faktorer, men även bildkvalitet kan studeras genom en bildrekonstruktion. Ett program för detta är CASToR, utvecklat för att återskapa bilder inom området för medicinsk bildvetenskap. Med dessa verktyg för simulering och bildrekonstruering kan arbetet för utveckling och förbättring inom området för PET-verksamheten fortskrida.

1 Abbreviations

BGO - Bismuth germanate oxide

CASToR - Customizable and Advanced Software for Tomographic Reconstruction

FDG - Fluorodeoxyglucose

FOV - Field of view

FWHM - Full width at half maximum

GATE - Geant4 Application for Tomographic Emission

LEHR - Low-energy high-resolution

LSO - Lutetium oxyorthosilicate

LOR - Line of response

LYSO - Lutetium yttrium oxyorthosilicate

ML-EM - Maximum-likelihood expectation maximization

OGL - Open Graphics Library

OGLIX - OpenGL ImmidiateX

OGLSX - OpenGL StoredX

OSEM - Ordered subset expectation maximization

PET - Positron emission tomography

PDF - Probability density function

PMMA - Polymethyl methacrylate

PMT - Photomultipler tube

SNR - Signal-to-noise ratio

Contents

2   Introduction

Positron Emission Tomography (PET) is a diagnostic tool used in the field of nuclear medicine in order to study the functionality of a patient, for example, cell metabolism. PET detects the two photons created from the annihilation of a positron, originating from the decay of a radioactive substance. If the two photons are detected within a short timing window a line between them is drawn and the decay is assumed to have occurred somewhere along this line, this is called a coincidence. By collecting a sufficient amount of coincidences a final image can be reconstructed, providing necessary information regarding body functionality. PET has evolved over the last couple of decades, now playing a vital role in the healthcare system as a tool for cancer diagnosis [1].

The field of nuclear medicine is always in need of improvement and optimisation of equipment and exam protocols. To do so, understanding how scanner geometry and the underlying processes affect the final result is thus of uttermost importance. A good tool used to gain a better understanding of the system as a whole is Monte Carlo simulations. The Monte Carlo method is a statistical tool that utilises random numbers to solve complex problems. A Monte Carlo simulation may to some degree be advantageous to measurements, for example, one does not have to construct a prototype of a scanner to investigate how detector geometry and composition will affect the result [2].

2.1   The Aim

PET is an important tool for diagnosing certain tumours and has a vital role in todays health care system. Therefore, there exists a desire in being able to model realistic clinically available PET systems. GATE is a software, dedicated towards emission tomography, that utilizes the Geant4 kernel in order to, in a simplistic way, model comprehensive scanner geometries, and with well-validated physics simulate particle propagation. GATEs user-friendly way of setting up the simulation and together with its unique feature of being capable of handling time-dependent processes allows for coherent and realistic simulations. GATE can be used as a tool for improvement and optimisation, and then, the first and foremost question becomes whether or not the simulated data can be trusted.

The aim of this thesis was to gain an understanding of the Monte Carlo method, GATE, and the image reconstruction software CASToR and testing their validity. This was done by simulating a human-like realistic phantom with an activity distribution similar to that of a clinical exam using 18F-fluoride in a modeled PET system using the GATE Monte Carlo software. Measurements and simulations of the NEMA body phantom were also performed. Data acquired from the simulations were reconstructed with CASToR. Comparisons between simulated results and measured were performed to test the validity of GATE and CASToR. Evaluations between different imaging systems, namely, PET and Single Photon Emission Computed Tomography (SPECT) were performed as part of the thesis. This was done by comparing PET and SPECT simulations of identical phantoms source distribution.

3 Background

3.1 The positron decay

The positron, the electron anti-particle, is produced either by pair-production or by a nuclear decay, specifically the β^+-decay. Usually, β^+-decays occurs in atoms with an abundance of protons, the atom will gain stability by converting a proton to a neutron and the positive charge is transferred away from the site of decay along with the positron. As the positron traverses in the surrounding media it loses kinetic energy either through inelastic collision with orbital electrons or through inelastic collision with nuclei. Once the positron approaches zero thermal energy an annihilation with an electron will occur, in the process creating two photons with an energy of 511 keV each [3]. The annihilation photons will be emitted with an angle of 180° with respect to one another. In the case that the positron has not completely lost all its energy whilst interacting with an electron a phenomenon, know as annihilation in flight, will occur resulting in a small deviation from the 180° emission angle between the two photons, called acollinearity.

In table 1 are some relevant parameters of commonly used β^+-emitting radionuclides shown [3].

Table 1: Some typical β^+-emitters and some of their characteristics [3].

Radionuclide	Half-life [min]	Maximum positron energy E_{max} [keV]	Maximum range in water R_{max} [mm]
^{11}C	20.4	0.959	4.1
^{13}N	9.96	1.197	5.1
^{15}O	2.03	1.738	7.3
^{18}F	109.8	0.633	2.4
^{68}Ga	68.3	1.898	8.2

3.2 PET - Physics

An essential part of nuclear medicine is imaging. PET is a tool used to visualise body functionality, for example, cellular metabolism and blood flow.

To obtain PET-data a labeled compound, called radiotracer, must be injected and distributed in the studied subject. Different radiotracers are used for different types of exams, where for example fluorodeoxyglucose (FDG) is widely used to examine certain types of tissue metabolism [4]. The radiotracer is distributed according to the functionality of the subject, accumulating high or low concentration of radiotracer in areas with abnormal performance. The radiotracer will decay, emitting positrons and eventually, the creation of annihilation photons will take place. The PET camera geometry typically consists of sectors of scintillator crystals in blocks coupled to electronic readout components like photomultiplier tubes (PMT). The segments of sectors are repeated so

that several rings of detectors are created. The crystals are often made of bismuth germanate oxide (BGO), Lutetium oxyorthosilicate (LSO) or Lutetium yttrium oxyorthosilicate (LYSO). The crystals used in PET scanners should desirably be made of materials with properties of high density and effective atomic number, high light output and short decay constants [5]. The cylindrical geometry of the scanners provides a good detection efficiency of the two annihilation photons produced from the positron-electron annihilation. If the annihilation photons are detected in coincidence, within a specific timing window period (usually in the order of nanoseconds), a line of response (LOR) can be defined. The LOR is defined between the two detectors in which the photons generated a signal and is considered valid only if a few criteria are met. One criterion is the previous mentioned, that the detection in coincidence has to be within a set timing window. Another criterion is that the LOR has to have occurred within a valid acceptance angle. Lastly, if the LOR is to be considered valid the two detected photons both have to have an energy within a pre-selected range. The LOR is an indication that somewhere along this defined line a decay of the radiotracer, or more correctly, the annihilation has occurred. This is not completely true, in fact, PET is affected by several different types of coincidence events: true, random, scattered, multiple and prompt gammas [5]. A true coincidence event originates from a single annihilation and is absorbed in the detector crystal without any other interactions. A random event occurs due to an accidental detection of two unrelated events within the timing window. Scattered events are true events that have undergone Compton scattering before entering the detector. Collectively, all different kinds of coincidence events that meet the criteria of producing valid LORs are called prompts. Figure 1 illustrates a true, scattered and random coincidence event.
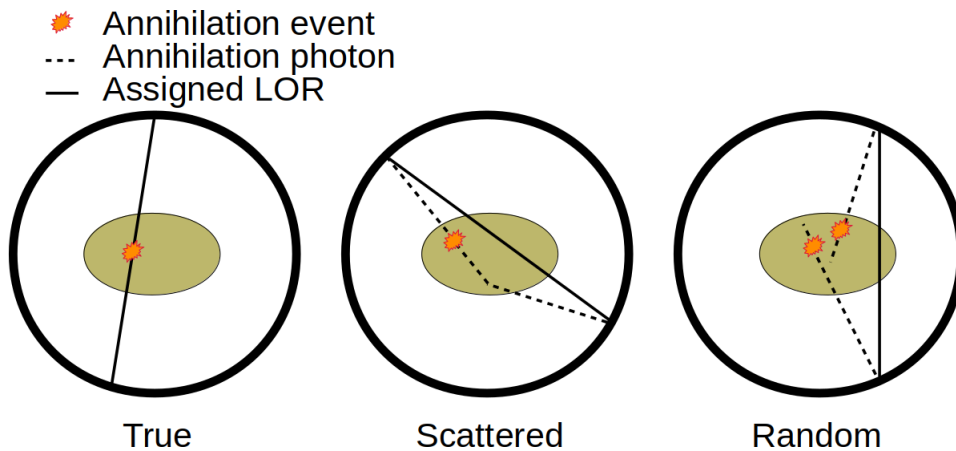

Figure 1: The depiction of the different kind of available prompts.

Both random and scattered events affect the image contrast and resolution negatively. Random coincidences add uncorrelated data to the image, decreasing the image contrast. The rate at which random coincidences are detected is estimated as

$$R_{i,j} = 2\tau n_1 n_2, \tag{1}$$

3

where τ is the coincidence timing window, n_1 and n_2 are the rate of detection of single-photon events of detector 1 and 2 respectively (under the assumption that there exist no correlation between n_1 and n_2). From equation (1) one can see that by decreasing the coincidence timing window one would accept fewer random events to the data, but at the same time by decreasing the timing window one would also decrease the rate at which true events are detected. This relation between true and randoms forces a trade-off between sensitivity and image degradation. Scattered events will also impact image quality by wrongly positioning the LOR. The degree to which scatted coincidences affect the image depends on activity distribution, the size of the source and the surrounding media composition [5]. Other factors affecting the image quality is the physical properties of the positron. As the generated positron will travel a distance before losing enough kinetic energy to be annihilated makes the positioning of the site of decay uncertain. This uncertainty depends on the range of the positron in the given media, ultimately setting a maximally obtainable spatial resolution. Acollinearity also affects the resulting image due to the LOR not exactly passing through the site of decay, resulting in a mispositioning of the LOR, effectively degrading the spatial resolution.

The number of detected prompts will be proportional to the activity of the radiotracer. It is thus important when performing quantitative analysis that the PET-data have been corrected for unwanted coincidences. One should also correct for the effect of attenuation [6]. This can be done by the following relation, the measured number of prompts, P, are connected to the number of true events, T, by the relation

$$P = N(AT + S + R), \tag{2}$$

where N, A, S, and R are the normalization, random, scatter and attenuation correction factors [6].

The goal of PET has become to detect deviations from normal radiotracer distribution by forming an image using the coincidences detected by the scanner - all while still being minimally non-invasive.

3.3   PET - Reconstruction and imaging

Constructing an image from acquired projections can be explained as a linear inverse problem. Suppose there exist an image-vector f representing the unknown activity distribution, the matrix A describes the imaging system and the vector p contains the collected set of PET-projections. The imaging process can then be modeled as the following,

$$p = Af. \tag{3}$$

The central slice theorem plays a vital role to tomographic reconstruction, this theorem states that the one-dimensional Fourier transform of projections acquired at a certain angle θ is equivalent to a radial line at the same angle θ through the center of the two-dimensional Fourier transform of the image. The cornerstone of reconstructing images relies on Fourier analysis. The implication of tomographic reconstruction narrows down

to the task of measuring the projections of image f for all angles of $\theta \; \epsilon \; [0,\pi]$. Sampling over this interval will result in radial lines sweeping across the whole Fourier domain. However, there are practical limitations to measuring every single projection over the span of $[0,\pi]$, as collecting radial lines in the Fourier domain will be a circular representation, and the way data is handled is performed through quadratic matrices, thus as the radial lines sweeping across the Fourier domain, higher frequencies will not be sampled as tightly as the low frequencies - meaning the depiction of high-frequency objects may be distorted, or in some cases completely vanish. In order to avoid this problem, as already mentioned, sampling across every single angle over the span of $[0, \pi]$ is required, although not practically possible. To some degree, one can say that sacrificing higher frequencies is done to make tomographic reconstruction clinically possible. Lastly, an inverse Fourier transform of all the radial lines will result in the final image.

Formulating the imaging model as equation (3), as an analytical formulation, assumes the data being deterministic to its nature, containing no statistical noise. The analytical formulation is solvable directly and the result is obtained very fast since the image vector f can be obtained directly from the projections p. However, data acquired through PET physics contains plentiful processes that inherently are stochastic to its nature and thus modelling the data as analytical without any stochastic degrading factors will lead to a limitation of quantitative accuracy. For example, the analytical reconstruction methods do not model degrading factors in PET systems such as the positron range and acollinearity, and secondly, the analytical method cannot take stochastic variability of photon detection into account [6].

Statistical reconstruction can be used to improve the model by including statistical noise, however by doing so an increased complexity of the reconstruction problem emerges. A unique solution of equation (3) can no longer be obtained directly due to the presence of noise - the solution is instead obtained iteratively, meaning the solution is progressively updated to an improved result. The approach of the iterative method usually goes as follows:

(1) An initial guess of the activity distribution is made.

(2) The estimated projections are then calculated by forward projecting the initial guess.

(3) The calculated projections are compared to the measured projections. The projections are back-projected and then adjusted for according to a set criterion.

The initial estimate will always be far from the optimal solution, however, as the process is repeated by reiterating step (2) and (3) the best estimation of the solution will eventually be obtained [6]. Importantly, one needs to know what the desired solution is, or alternatively, what the 'best' solution is. The criterion used to find the 'best' image is often represented as a cost function which measures the similarity between the guessed and measured image. A widely used criterion is the maximum likelihood approach or the ordered subset method. The outcome of using iterative methods is often

advantageous to the analytical method as the final result enjoys better quality features in addition to a more accurate estimation of tracer concentration, improved image contrast, better spatial resolution and improved noise properties [3].

3.4   The Monte Carlo Method

The essential idea of Monte Carlo simulations is to solve deterministic problems using randomness. The Monte Carlo method is a statistical tool that utilises randomly generated numbers as the foundation to perform simulations. To successfully perform a Monte Carlo experiment the system and its inherent attributes have to be accurately described and modeled after known probability density functions (pdf) [2]. The pdf describes the probabilty that a set of interactions for a given system will occur [7]. This characteristic of the Monte Carlo method enables the study of underlying effects or processes of complex systems such as radioactive decay and particle propagation since all details are made accessible from the simulation. However, in order to obtain results with reasonable statistical uncertainty, the pdf has to be sampled extensively [2], so in the case of particle propagation, many trajectories have to be sampled, which can result in the simulation taking a long time to be completed.

The Monte Carlo method uses random numbers extensively to control the decision making of the very next step or event in a simulation, thus a fundamental and extremely important part of the Monte Carlo simulation is the production of random numbers. However, true randomness cannot be obtained from calculations and must be produced by a random process, such as radioactive decay. True randomness cannot be calculated because they are randomly distributed, in the process making them per definition unpredictable [8]. For practical considerations, pseudorandom numbers produced by computer algorithms can be used to generate uniformly random numbers. Pseudorandom numbers are not truly random, but given a sequence of numbers, calculated from random seed numbers, are suppose to appear as random [2, 8]. Two important traits that a random number generator desirably should have are

(1) Good random distribution - good randomness of the generated numbers.

(2) Long periods of numbers - the sequence does not continue infinitely, after a finite set of numbers the sequence will restart.

It is important to note that using the same seed twice will result in the same sequence of numbers, meaning two simulations will end up identical.

The Monte Carlo method is a useful tool in medical imaging. It is not always practical neither possible to perform an experimental study, and in those cases, a simulation could act as an alternative. The rise of specific Monte Carlo simulation software such as SimSET [9], SIMIND [10] and GATE [11] may have even made simulation studies advantageous in some aspects to the experimental ones as it is easy to tweak different parameters in a Monte Carlo simulation without having to change the initial set-up. This makes Monte Carlo simulations an excellent tool for the ever-present goal of improving,

developing and optimising new methods and protocols within the field of medical imaging.

3.5   Geant4

To handle an ever-growing issue regarding increased demand for accurate and comprehensive physics simulations Geant4 was designed and developed - a general purpose Monte Carlo simulation toolkit. Geant4 offers the possibility to model a simulation geometry in different ways regarding shape, size, and material and by assigning these volumes sensitive elements allows for storing information from particle interactions. The physics is customisable, allowing the user to choose which physical processes are to be present in the simulation [12]. This way of customising the simulation gives the user complete control, allowing systems to be modeled for specific applications.

The geometry of Geant4 is made up of logical and physical volumes. A logical volume is an element represented by a certain shape, and this volume can in itself hold other volumes and their attributes. A physical volume will define the position or placement of a logical volume [12]. The positioning of a volume will be in relation to a mother volume, that is, an enclosed logical volume. This way of representing volumes allows the user to define their geometry set-up in a tree-like hierarchical structure, each sub-volume smaller than the previous. It is important to state that no overlaps between volumes are allowed (for example, a sub-volume may not surpass the dimensions of its parent volume) as the tracking and navigation system of Geant4 will not be stable in overlapping regions.

The tracking category of Geant4 is the main manager and contributor to the evolution of a track - a track is a snapshot of a particle in its current state. A physics process associated with a particle will propose a step - a step is the basic unit of a simulation. A step has two points, a start point and an end-point, each point containing information regarding its current physical parameters. Depending on the nature of the processes that invoked the step, the tracking category will contribute to determining a step length, generating secondary particles and make suggestions in changes to the state of the particle, for example killing the particle. The tracking, in other words, simply steers the invocation of processes, it scans all possible actions to decide how a step should be invoked. Information between the simulated particle and objects relevant to particle transportation, such as geometry and material are taken into considerations when a step is determined in order to accurately and realistically steer and step. A particle in flight is subjected to many competing interactions and processes, and in a realistic situation, a particle might travel through many regions, subjected to different materials before an interaction occurs. As mentioned, in Geant4 the particle is transported through steps, and it is therefore important that the decision making of how a particle's trajectory evolves is unbiased. In Geant4 this is done by calculating the distance to the point of interaction/decay, characterised by the mean free path λ. The probability that the particle will survive a distance l is given by

$$P(l) = e^{-n_\lambda},\tag{4}$$

7

where $n_\lambda = \int_0^l \frac{dl}{\lambda(l)}$. As the particle loses energy and changes discontinuously at volume boundaries it is important to keep in mind that λ will change during a step (note that a step is limited by a volume boundary, during the next step the particle logically belongs to the next volume, this is why no overlapping are allowed). The probability distribution of n_λ is an exponential, allowing us to set n_λ to

$$n_\lambda = -ln(\eta), \tag{5}$$

where η is a randomly distributed uniform number between [0,1]. It is this randomly generated number that Geant4 used to determine the distance to the point of interaction or decay in current material. Each newly produced particle or newly taken step will be given a new random number.

A hit is in Geant4 known as a snapshot of a physical interaction, or accumulation of physical interactions, that has occurred in a sensitive volume. Information regarding physical parameters is saved when they occur in these sensitive volumes. Every logical volume in the enclosing geometry can have a sensitive detector attached to it. The detector response can also be modeled allowing the hit to be processed to realistically mimic a detector output pulse - further improving the simulation model.

Geant4 offers the user a toolkit to simulate particle propagation in matter. Its versatile packages have made Geant4 applicable within the fields of particle physics, nuclear physics, and medical physics.

3.6 GATE - Geant4 Application for Emission Tomography

GATE is a Monte Carlo software, originally dedicated towards emission tomography applications, is built around the core of Geant4. The Geant4 kernel provides extensive and versatile Monte Carlo packages, with well-validated physics models [11], and allows the user to model complex and comprehensive geometries.

The design of a GATE simulation is declared in a way that the geometry, physics, radioactive source and so forth is set up using structural commands, each command performing a specific function. As Geant4 allows for both interactive and batched simulation, the commands can either be entered directly in the prompt after starting GATE, or, be called upon using a macro file (with the extension .mac). The macros are ASCII-files where a line contains a command to be executed, the order the commands are written in will determine the order in which the commands are interpreted by the prompt. Lines that start with a # will be seen as a comment. A macro file can call upon other macro files. To supply the user-friendly design of GATE the GATE commands are organised as a tree structure. All commands start with /gate/ followed by the specific area of the simulation being built, for example the command */gate/physics/addProcess Compton* refers to adding the physical process of Compton-interaction to the simulation. A complete simulation script should be defined in eight steps and the user should include the following:

(1) Visualisation parameters.

(2) Scanner geometry.

(3) Phantom geometry.

(4) Physical processes.

(5) Initialization of simulation.

(6) Detector modelling.

(7) Source(s).

(8) Random number generator and data output format.

Point (1) - (4) corresponds to a pre-initialization of Geant4, after point (5) no more changes to the geometry or the physics list can be made as the initialization triggers calculations of cross section tables. After point (8) the last thing to do is to declare the desired simulation time, and after that is done, the acquisition can be started.

The physics of GATE is available from the Geant4 kernel, containing models and corresponding cross-sections for interactions and decays of particles below 10 GeV. For sources used in PET such as ^{18}F and ^{11}C, GATE dedicates a module to generate the initial energy to the positron from a subsequent decay. This module uses the von Neumann algorithm [13] to randomly generate the positron energy according to appropriate β^+ spectra. The von Neumann module greatly increases the simulation speed by bypassing the radionuclide decay scheme provided by Geant4. These β^+ spectra of commonly used radionuclides have been parametrized in GATE based on the Landolt-Börnstein tables [14]. GATE also dedicates a module to account for acollinearity which is not included in Geant4.

The phantom in a GATE simulation can either be described as an analytical geometry or as a voxelized representation. The voxelized phantom should be assigned materialistic properties depending on its voxel values. Consider a situation where the phantom has the shape of a human torso, the voxels representing say, the heart, might have the values in the range of 10-20, those values should then be given the materialistic properties of a heart. Likewise, the source can either be analytical or voxelized. When using voxelized sources the user defines the amount of activity per voxel for a given voxel value. Consider the same situation as above, where the heart is defined by the voxel values 10-20. The activity of the heart is then assigned by setting a desired amount of activity to each voxel within the values 10-20, the cumulative activity will be the number of voxels in the range 10-20 multiplied by the set activity per voxel. This allows GATE to handle phantoms made from patient images and source distribution from clinical exams such that a highly realistic simulation can be performed.

The principle of particle propagation in GATE is as mentioned handled by the Geant4 kernel. An entire series of steps is a simulated trajectory (an event), and summarised an event will be carried out through the following three steps:

(1) The initial particle is produced or generated with its parameters.

(2) From the parameters, an initial step is calculated (that is, a the start- and end-point between interactions). During this step, changes to the particles parameters are calculated - and then updated.

(3) If a step occurs in volume with a sensitive detector attached to it, the information from the interaction is stored.

Step (2) and (3) are repeated until the energy of the particle is reduced below a certain threshold value or until the particle has left the enclosing volume.

Just like Geant4, GATE offers the possibility to model the digitizer, whose purpose is to simulate the electronic readout scheme. Simulating the electronic readout scheme allows the user to realistically mimic the detection process. The digitizer uses information generated in the sensitive detector and converts it into a signal - simulating the detector response and the processing performed by the scanner electronics. Apart from simulating the electronic readout, the digitizer also handles coincidence sorting in PET applications. When a particle interacts with a sensitive detector the hit is referred to as a single. The coincidence sorter opens up a timing window once a single is registered, and if another particle interacts within the timing window, in another detector, the coincidence sorting module will identify these two singles as a pair. These pairs will be grouped together and form a coincidence. Appropriately modelling the digitizer is important in order to properly and accurately reproduce the behaviour of certain imaging systems [11].

3.7 ROOT

ROOT is a framework developed at CERN for data processing and analysis. The ROOT file format is a powerful tool when one wants to access huge amounts of data quickly [15]. The ROOT format allows the user to save data and any C++ object in a compressed binary form including both the data and its description. In doing so ROOT does not have to handle data using an intermediate step of storing data in a text-file, compressing it and then interpret the compressed file. This frees up memory when storing and fetching data using the ROOT file format [15, 16]. The framework was developed for the purpose of handling huge amounts of data ever-present in the field of physics.

3.8 CASToR - Customizable and Advanced Software for Tomographic Reconstruction

CASToR is a software developed for tomographic image reconstruction. CASToR utilises iterative reconstruction algorithms to reconstruct SPECT and PET data [17]. As of today, analytical methods are not yet implemented. The PET datafile should be linked with its scanner geometry so that events can be coupled to the corresponding crystal pairs. CASToR utilises a scanner geometry integrity file (an ASCII file with characteristics unique to the scanner) to identify and give each detector element an identification number. This

identification number is used to identify all events that have occurred in the specific detector.

As mentioned in section 3.2, tomographic reconstruction can be formulated as an inverse problem, solving for the image vector. In CASToR the system matrix A is based on projectors. The task of the projector is to compute the system matrix elements corresponding to a given event. CASToR provides several different optimizers and projectors, amongst those the Maximum Likelihood Expectation Maximization (MLEM) algorithm. For each iteration, the following occurs

(1) The system matrix is computed by the chosen projector.

(2) The optimizer is called upon to update the data:

    (a) The current estimation of the image is forward projected.

    (b) Any estimation of background events is added.

    (c) Operations specific to the optimizer is performed to compute correction terms to the data.

    (d) Backward projection of the correction term in back-projected image.

A sensitivity image over all detection elements based on the scanner geometry description is required by the iterative optimization algorithms. The sensitivity image will be computed before the launch of iterations when reconstructing list-mode data.

CASToR provides utilities to directly convert a GATE simulation and the appurtenant macro to a CASToR file and scanner geometry integrity file respectively, provided that the ROOT format has been used.

4 Material and method

The features of GATE were used to build a model of a PET scanner and to simulate particle propagation. The modeled scanner was modeled with the G.E. PET/CT Discovery-690 as a template. The Discovery-690 was chosen as template because Skåne University Hospital has that model in their disposal. Bear in mind, the model does not fully represent that of a Discover-690 camera as parts such as shielding was not included.

These parameters were taken into considerations when modelling the PET camera.
Two main types of phantoms were simulated. One of the simulations consisted of a measurement of the NEMA 2012/IEC 2008 PET body phantom [18]. The measurement was carried out on the G.E. PET/CT Discovery-690 and the simulations were carried out on the modeled scanner. CT-images taken of the phantom were segmented to create the voxelized phantom used in the simulation. The simulations were performed on the modeled scanner described in section 4.1. Simulated data were reconstructed using the

CASToR software.

The other simulation consisted of simulating a phantom with highly realistic structures resembling that of a human body. The simulation consisted of simulating 18F-fluoride with an activity concentration and distribution similar to that of a clinical exam. The whole phantom was not simulated, instead, slices of the pelvic region was chosen. A tumour had also been randomly placed in the pelvic region. The simulated data were reconstructed using the CASToR software.

GATE version 8.0 was used together with Geant4 version 10.3, ROOT version 6.10.08 and CASToR version 1.2. Simulations were performed on a computer with Intel Xeon E5-1620 CPU and the operating system as the Debian based Linux distribution 64-bit Ubuntu 17.10.

4.0.1 G.E. PET/CT Discovery-690

The Discovery-690 has a cylindrical structure, with 24 detector rings, each ring containing 576 crystals, totaling to 13824 crystals. The crystals are made out of LYSO with the dimensions 4.2x6.3x25 mm^3. The tube has a transaxial field of view (FOV) of 70 cm and an axial FOV of 15.7 cm. The scanner has an energy window threshold of 425 keV and coincidence timing window of 4.9 ns.

4.1 Setting up a GATE PET simulation

When setting up the simulation the scripts were written with the steps mentioned in section 3.6 in mind. Description of how the phantom and source have defined has been saved for each subsection explaining that specific task, those parts can be found in section 4.3 and section 4.2.

Defining the visualisation parameters will not be mentioned further rather than it allows for easier modelling and handling of structures. GATE provides the user with several visualisation tools, the one used here was the Open Graphics Library (OGL). Note, in order to display a voxelized phantom the OpenGL StoredX (OGLSX) viewer does not work, instead, a viewer like OpenGL ImmidiateX (OGLIX) has to be used. A material file was read into GATE making it possible to assign volumes materialistic properties. The dimensions of the enclosing logical volume were declared and given the dimensions {x,y,z} = {1,1,1} m.

4.1.1 Geometry modelling

Inside the enclosing logical volume, a first system defining the hierarchical modality-specific structure was defined, a cylinder. The cylinder was given an inner diameter of 700 mm, an outer diameter of 810 mm and a tube length of 157 mm. The default position of the enclosing volume's daughter (the cylinder) is at the origin of the enclosing volume (that is, {x,y,z} = {0,0,0}). A daughter volume to the cylinder, a rotational sector, was then

defined with shape of a rectangle and with the dimensions {x,y,z} = {55.0,37.8,157} mm. The rotational sector was then moved 377.5 mm in the x-direction to place the sector inside the walls of the cylinder. In the rotational sector a module was created in the shape of a rectangle with the dimensions {x,y,z} = {55.0,37.8,37.8} mm. As the daughter is created at the center of its parent volume the module was not needed to be translocated. A crystal was then created as a daughter to the module and was given the dimensions {x,y,z} = {25.0,4.2,6.3} mm. The crystal was then moved as close as possible to the inner wall of the cylinder without exceeding its dimensions. The crystal was given a daughter, a layer, which was given the name 'LYSO' with the same dimensions as the crystal. All volumes were assigned the material air except the layer which was assigned the material LYSO.

The following structural commands show the process of setting up the scanner geometry mentioned above.

```
/vis/open OGLIX
/vis/viewer/set/viewpointThetaPhi 60 60
/vis/drawVolume
/gate/geometry/setMaterialDatabase /path/to/database
/gate/world/geometry/setXLength 1.0 m
/gate/world/geometry/setYLength 1.0 m
/gate/world/geometry/setZLength 1.0 m
```

```
/gate/world/daughters/name cylindricalPET
/gate/world/daughters/insert cylinder
/gate/cylindricalPET/setMaterial Air
/gate/cylindricalPET/geometry/setRmax 405 mm
/gate/cylindricalPET/geometry/setRmin 350 mm
/gate/cylindricalPET/geometry/setHeight 157 mm
/gate/cylindricalPET/placement/setTranslation 0 0 0
```

```
/gate/cylindricalPET/daughters/name rsector
/gate/cylindricalPET/daughters/insert box
/gate/rsector/setMaterial Air
/gate/rsector/geometry/setXLength 55 mm
/gate/rsector/geometry/setYLength 37.8 mm
/gate/rsector/geometry/setZLength 157 mm
/gate/rsector/placement/setTranslation 377.5 0 0 mm
```

```
/gate/rsector/daughters/name module
/gate/rsector/daughters/insert box
/gate/module/setMaterial Air
/gate/module/geometry/setXLength 55 mm
/gate/module/geometry/setYLength 37.8 mm
/gate/module/geometry/setZLength 37.8 mm
/gate/module/placement/setTranslation 0 0 0 mm
```

```
/gate/module/daughters/name crystal
/gate/module/daughters/insert box
/gate/crystal/setMaterial Air
/gate/crystal/geometry/setXLength 25 mm
/gate/crystal/geometry/setYLength 4.2 mm
/gate/crystal/geometry/setZLength 6.3 mm
/gate/crystal/placement/setTranslation -15 0 0 mm
```

```
/gate/crystal/daughters/name LYSO
/gate/crystal/daughters/insert box
/gate/LYSO/setMaterial LYSO
/gate/LYSO/geometry/setXLength 25 mm
/gate/LYSO/geometry/setYLength 4.2 mm
/gate/LYSO/geometry/setZLength 6.3 mm
/gate/LYSO/placement/setTranslation 0 0 0 mm
```

Using the command */gate/geometry/rebuild* allows the geometrical structures that have been defined to be updated in any of the available OGL viewers. Figure 2 shows the different parts of the geometry being implemented by the structural commands. The solid part of the subfigures (a) - (e) in figure 2 represents the part of the scanner being modeled at that time.

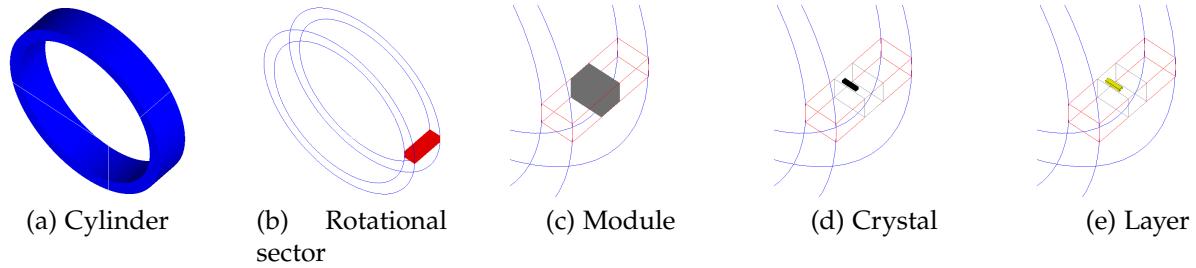| (a) Cylinder | (b) Rotational sector | (c) Module | (d) Crystal | (e) Layer |

Figure 2: Solid shape indicates what part of the scanner geometry at that current subfigure is being modeled. Note that images (c) - (e) have been magnified for visual purposes.

The G.E. PET/CT Discovery-690 contains 13824 crystals divided over 24 rings [19]. To solve this GATE uses repeaters so that every 13824 crystal does not have to be added one by one. The crystal was repeated 54 times in each module, 9 in the y-direction and 6 in the z-direction. The modules were then repeated 4 times in z-direction inside the rotational sector. Since the crystals have already been repeated in the module and the module is repeated in its current state, all the sub-volumes within the module will accompany the repeated module.

The following commands show the crystal and module being repeated.

```
/gate/crystal/repeaters/insert cubicArray
/gate/crystal/cubicArray/setRepeatNumberX 1
/gate/crystal/cubicArray/setRepeatNumberY 9
/gate/crystal/cubicArray/setRepeatNumberZ 6
/gate/crystal/cubicArray/setRepeatVector 0 4.2 6.3 mm
```

```
/gate/module/repeaters/insert cubicArray
/gate/module/cubicArray/setRepeatNumberX 1
/gate/module/cubicArray/setRepeatNumberY 1
/gate/module/cubicArray/setRepeatNumberZ 4
/gate/module/cubicArray/setRepeatVector 0 0 37.8 mm
```

The *setRepeatVector* command indicates the distance each repetition should be moved. Figure 3 shows the updated geometry after the crystal and module had been repeated.

14

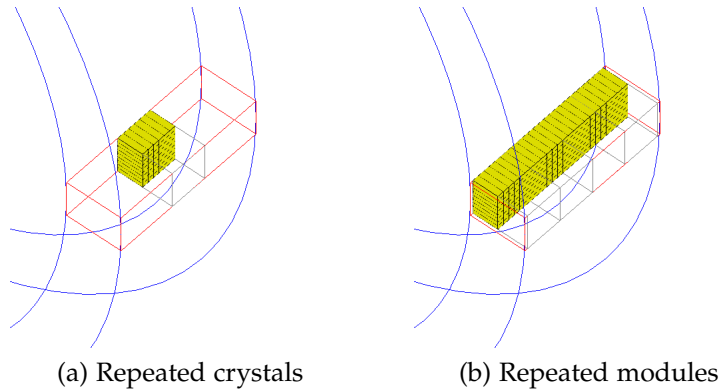(a) Repeated crystals   (b) Repeated modules

Figure 3: Crystals and modules repeated inside a rotational sector.

Lastly, the rotational sectors were repeated in a ring-like manner 64 times. The following two commands show how the sectors were repeated. Note, when using a ring repeater the *setRepeatVector* should not be declared.

```
/gate/rsector/repeaters/insert ring
/gate/rsector/ring/setRepeatNumber 64
```

The final resulting geometry of the modeled scanner can be seen in figure 4. Once the crystals have been repeated in the module the repetition of modules will include the repeated crystals, in fact, any daughter volume inherent in a mother volume will accompany the mother volume if repeated - it is, therefore, important to repeat the daughter volumes first, working upwards in the hierarchy.
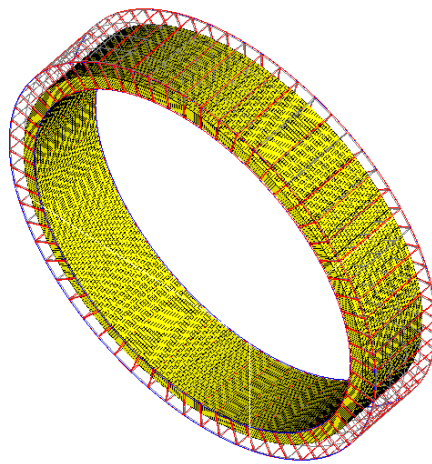

Figure 4: The repetition of the rotational sectors, resulting in a cylindrical PET scanner geometry containing 24 rings constituted of 576 LYSO crystals in each ring.

15

The crystals were attached a sensitive detector so that hits in those regions could be stored and processed.

4.1.2 Setting up the physics

Physical interactions relevant to positron emitters were defined. Included interactions were the photoelectric effect, Compton scattering, Rayleigh scattering, bremsstrahlung, multiple electron/positron scattering and electron/positron ionisation. The physics were modeled with the standard package from Geant4 which relies on the parametrisation of experimental data and is appropriate for processes between 1 keV and 100 TeV. In order to avoid infrared divergence cuts were applied to charged particle processes. Cuts will stop the production of secondary particles below a certain threshold limit. No reduction techniques were applied to the simulation.

4.1.3 Finalizing the simulation

The energy window was set with a threshold of 425 keV, an uphold of 750 keV and crystal energy resolution for LYSO crystal was set to 8%*. The coincidence timing window was set to 4.9 ns. The output format was chosen to be ROOT and JamesRandom was chosen as the random number generator. The random number generator seed was set to *'auto'*, which uses the computers system clock to choose starting seed.

In NEMA simulation 1, the energy threshold was set to 300 keV and the crystal energy resolution was set to 20%.

4.2 NEMA phantom

The NEMA 2012/IEC 2008 body phantom for PET applications was used to perform a measurement, displayed in figure 5.
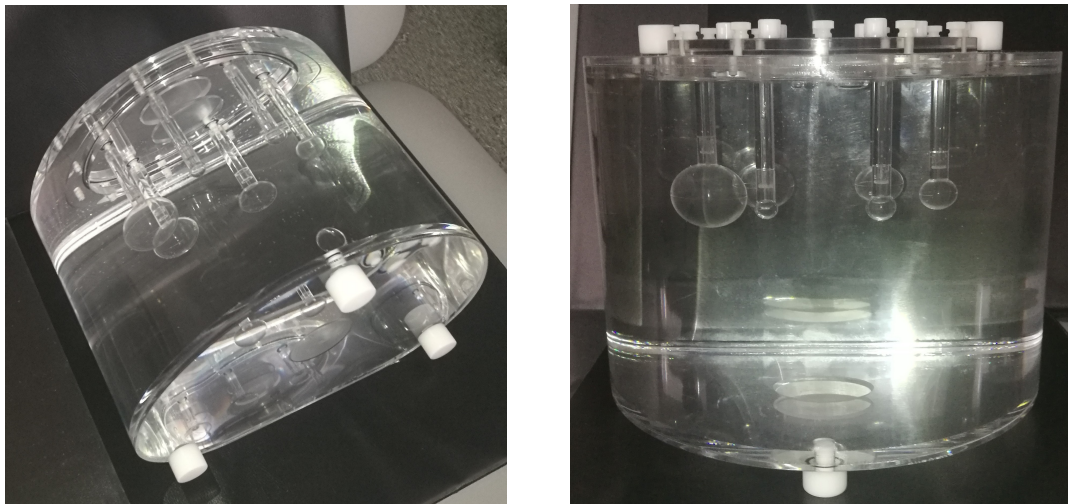

Figure 5: Images of the NEMA 2012/IEC 2008 body phantom.

The phantom is a D-shaped cylinder with the dimensions 24.1x30.5x24.1 cm^3, and a disposable volume of 9.7 L. The phantom contains six fillable spheres with inner diameters of 37, 28, 22, 17, 13 and 10 mm.

The background activity was set to zero while the activity concentration in the spheres was set to 836 kBq/ml of 18-F, totaling to 40 MBq. The measurement was carried out on a G.E. PET/CT Discovery-690 at Lund University Hospital. The data was collected in list-mode, allowing the data to be reconstructed (with the G.E. VUE Point HD algorithm) at any elapsed measured time.

CT-images acquired from the measurement were segmented into a voxelized phantom, the segmentation was performed in MATLAB. The matrix dimensions were cropped to 301x301x83 (original matrix size: 512x512x83) with the voxel size {x,y,z} = {1.37,1.37,3.75} mm. The segmented NEMA-phantom was assigned materialistic properties and was then inserted into the scanner geometry, figure 6. The voxelized phantom was assigned the same activity concentration in the spheres as the activity concentration used in the measurement. The acquisition time was set to 120 seconds.
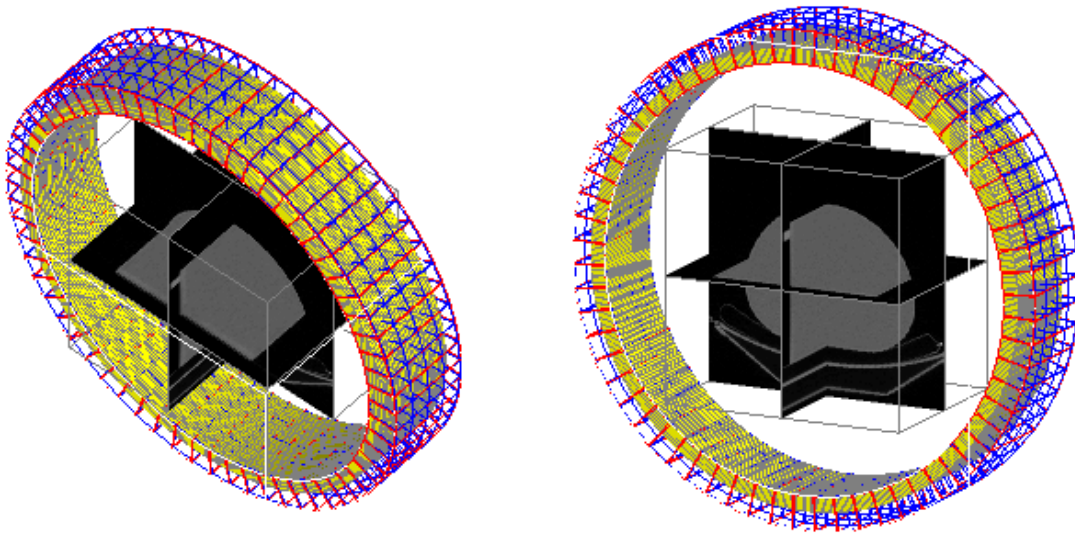

Figure 6: The segmented NEMA-phantom inserted into the simulating geometry. The two images depict the same situation with different visualisation viewpoints.

The resulting ROOT file was then converted to a corresponding CASToR file with the conversion tool *castor-GATERootToCastor*. The scanner geometry integrity file was created from the GATE macro by providing the input *-geo* during the conversion from ROOT to CASToR file. A map with attenuation properties (given in cm^{-1}) was created in MATLAB with the same dimensions as the simulated phantom. The data was reconstructed with the ordered subset expectation maximization (OSEM) method using 8 iterations and 8 subsets. The images were reconstructed to the same matrix dimensions as the images from the measurement, those being 192x192x83 with a voxel size of {x,y,z} = {3.65,3.65,3.27} mm. The castor-GATERootToCastor inputs are displayed below,

```
castor-GATERootToCastor -i/-il PETSIM_NEMA.root -o SIM_NEMA -m MyNema-
Macro.mac -geo -s My_Nema_Pet
```

where -i/-il specifies the input ROOT file/files, -o specifies the output name of the CAS-
ToR file, -m specifies the input GATE macro file, -geo generates a scanner geometry
integrity file from the provided GATE macro file and -s specifies which file the geometry
integrity file is.

Below are the castor-recon inputs displayed,

```
castor-recon -df SIM_NEMA_CstrProj.Cdh -atn AttMapNema.hdr -it 8:8 -dim
192,192,83 -vox 3.65,3.65,3.27 -fout ReconstructedImageNema
```

where -df specifies which CASToR file to be reconstructed, -atn includes the attenuation
map when computing the system matrix, -it 8:8 specifies the number of iterations and
subsets, -dim specifies the dimensions of the reconstructed image, -vox specifies the size
of a voxel and -fout declares the name of the reconstructed image.

Two different NEMA simulations were performed. The first with the energy window
set to 300 - 750 keV and a crystal energy resolution of 20% (NEMA simulation 1). The
second simulation was performed using the settings mentioned in section 4.1.3 (NEMA
simulation 2). The second NEMA simulation was simulated 64 seconds due to lack of
remaining time.

4.3   Realistic human-like phantom

A highly realistic human-like voxelized phantom, the XCAT phantom [20], with the
dimensions 148x148x41 was created of the pelvic area. The size of the voxels were {x,y,z}
= {2.8,2.8,2.8} mm. Codes corresponding to certain parts of the voxelized phantom were
assigned specific materialistic properties corresponding to that of a human. The activity
concentration and distribution of the voxelized phantom were supposed to resemble that
of a clinical exam. The premise for a clinical exam activity was that the base of sacrum
should have an activity concentration of about 13 kBq/ml, the rest of the voxels (activity
concentration) were scaled appropriately according to an activity distribution file. The
phantom was then inserted into the simulation geometry, figure 7. The acquisition time
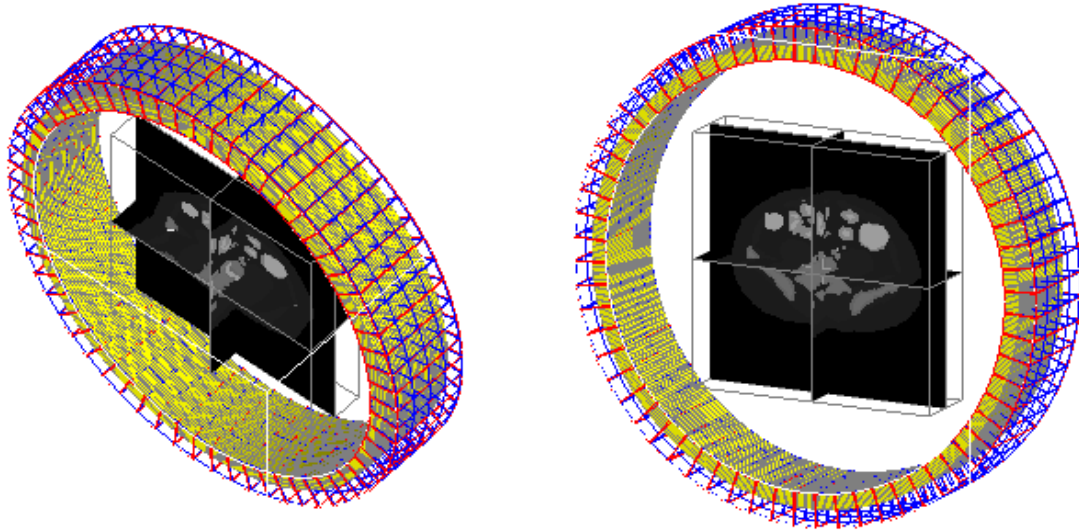was set to 120 seconds.

Figure 7: The XCAT phantom inserted into the scanner geometry. The two images depict the same situation with different viewpoint settings in the OGLIX viewer.

The resulting ROOT file was converted to a corresponding CASToR file with the conversion tool *castor-GATERootToCastor*, provided by the CASToR software. The images were reconstructed with the same dimensions as those of the original phantom (a 148x148x41 matrix with voxel size {x,y,z} = {2.8,2.8,2.8} mm). The castor-GATERootToCastor inputs are displayed below,

```
castor-GATERootToCastor -i/-il PETSIM.root -o SIM -m MyMacro.mac -geo -s My_Pet
```

Displayed below are the castor-recon inputs.

```
castor-recon -df SIM_CstrProj.Cdh -atn AttMap.hdr -it 8:8 -dim 148,148,41 -vox 2.8,2.8,2.8 -fout ReconstructedImage -conv 4.,4.,3.5::psf -conv 6.,6.,3.5::post
```

Due to the presence of noise, the projections were filtered with a Gaussian kernel, the *-conv* option. The first input declares the transaxial FWHM, the second input declares the axial FWHM and the third input states the number of sigmas to be included (the different inputs in that order are separated by a comma).

The reconstructed images were visually compared to the result of an 18F-fluoride clinical exam acquired with a Philips Gemini TF PET/CT camera. Available 18F-fluoride images taken with the Discovery-690 were not patient study images, the images were thus not permitted to be used without restrictions applying. Therefore the XCAT comparison was made with images taken with a Philips Gemini TF PET/CT instead of a G.E. PET/CT Discovery-690.

4.3.1 An example of Monte-Carlo-based evaluation of imaging systems

At Skåne University hospital, there is a general interest to quantify the tumor burden of metastatic skeletal malignancies by the use of quantitative measures, such as the bone scan index [21]. This procedure to quantify the number and extent of lesions can be made by both SPECT and by PET investigations, and where the latter has a better spatial resolution which could be a beneficial property for the quantification procedure. In order to evaluate the difference for a realistic radionuclide distribution, one way could be to do Monte-Carlo evaluations using accurate models of a SPECT and a PET system for an identical distribution. The following example described such a comparison between SPECT and PET models and is a research that is planned for in the future.

Since the digital phantom has been used to simulate a PET acquisition with GATE, the same phantom was used (with the same source distribution) to simulate a SPECT acquisition. The purpose was to get a glance over differences and similarities between PET and SPECT regarding spatial resolution. Thus, comparisons of GATE reconstructed images were made with a SIMIND SPECT simulation of ^{99m}Tc-HDP (hydroxydiphosphonate) of the same phantom (the matrix dimension of the phantom was changed to 128x128 with a voxel size of 4 mm^3).

SIMIND is a Monte Carlo code written in FORTRAN, dedicated to simulating a SPECT scintillation camera. In the Monte Carlo code of SIMIND photons are emitted from an activity distribution within a phantom. The emitted photons are followed step by step, with details of the photon history stored, towards the camera. If a photon is passing through the collimators and into a scintillation crystal then the photon is explicitly followed until it has escaped the crystal or is absorbed. SIMIND offers the possibility to simulate different collimators.

The camera used in the SIMIND simulation geometry was a Siemens with NaI(Tl) crystal (crystal thickness 9.525 mm and energy resolution 9.5% FWHM at 140 keV) with an energy window centered around 140 keV with a width of 15%. A low-energy high-resolution (LEHR) collimator was chosen. The acquisition was collected in a 360-degree rotation using 120 projections, each projection collected for 15 seconds. A non-circular orbit was simulated to calculated the distance from the phantom boundary to the collimator surface of each projection angle. For a clinical realistic SPECT exam it was assumed that 600 MBq was present in the whole phantom, and since only the pelvic region was used in the simulation the activity 203 MBq was set in that region as it is estimated that 60% of the activity is accumulated in the bones and that the exam is normally started three hours after injection. Poisson distributed noise was added to the projection data after normalisation to the correct activity and acquisition time.

The SIMIND simulated data was reconstructed with the CASToR software after conversion from SIMIND format to CASToR format. 8 iterations and 8 subsets were used (15 projections per subset). An attenuation map was included during the reconstruction, the map was produced by features present in the SIMIND code. Because of the presence of

noise in the SPECT projections the reconstructed images were filtered with a Gaussian kernel with a sigma of 0.9.

4.4   Data evaluation - NEMA

Data acquired from both the measurement and simulation were processed in a few different ways. For the measurement, information regarding the number of prompt-, scattered-, and random events were acquired from the DICOM tag. The CASToR conversion tool computes the respective number of prompts, trues, scatters and randoms from the ROOT meta-data.

The true fraction, TF, was calculated as

$$TF = \frac{T}{P},$$

(6)

where T is the number of true events and P is the number of prompts.

The scatter fraction, SF, was calculated as

$$SF = \frac{S}{P},$$

(7)

where S is the number of scattered events.

The random fraction, RF, was calculated as

$$RF = \frac{R}{P},$$

(8)

where R is the number of random events.

The system sensitivity, S_{sys}, was estimated as

$$S_{sys} = \frac{P}{t \cdot A},$$

(9)

where t is the acquisition time and A is the total activity. The sensitivity is given in cps/kBq.

An intensity profile was drawn over the center of three spheres of both the images from the measurement and the images from the simulation, the profiles can be seen in figure 9. The FWHM was obtained from the intensity profiles using linear interpolation. The data were normalized to the maximum value in the profile.

5 Results

5.1 NEMA

Images from the measurement and reconstructed simulated data can be seen in figure 8. All the images have been reconstructed using 8 iterations and 8 subsets.

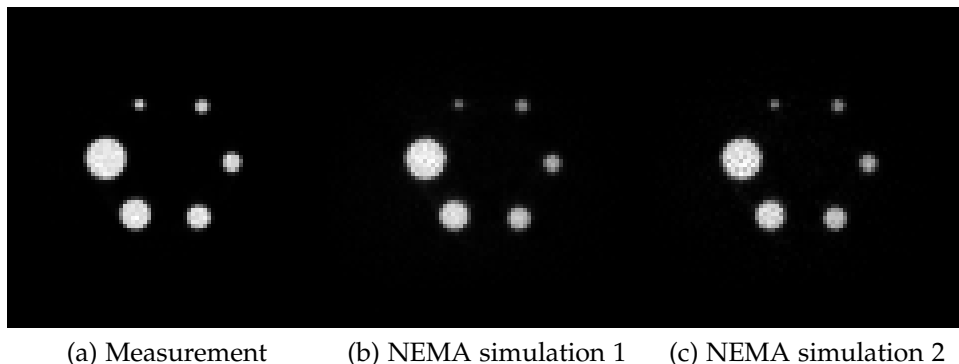(a) Measurement   (b) NEMA simulation 1   (c) NEMA simulation 2

Figure 8: Images from measurement and simulations.

Table 2 shows the number of prompts, trues, scattered and randoms obtained from the measurement and the simulations. The measurement and NEMA simulation 1 acquired data for 120 seconds while NEMA simulation 2 acquired data for 64 seconds. NEMA simulation 1 corresponds to the simulation with the energy window being 300 - 750 keV and crystal energy resolution 20% while NEMA simulation 2 represents the settings defined in section 4.1.3.

Table 2: The number of prompts (P), true (T), scatter (S) and random (R) events.

	Measurement (120 s)	NEMA simulation 1 (120 s)	NEMA simulation 2 (64 s)
P [1]	24340226	40262382	10153241
T [1]	15498123	11511446	4735923
S [1]	5526650	17992814	3231077
R [1]	3315454	10758122	2186241

The true-, scatter-, and random-fractions are displayed in table 3.

Table 3: True-, scatter- and random-fraction calculated with equation (6), (7) and (8) respectively.

	Measurement (120 s)	NEMA simulation 1 (120 s)	NEMA simulation 2 (64 s)
TF [1]	0.64	0.29	0.47
SF [1]	0.23	0.45	0.32
RF [1]	0.14	0.27	0.22

The system's sensitivity estimated with equation (9) for a 120 second time period resulted in 5.1 cps/kBq for the measurement and 8.3 cps/kBq for NEMA simulation 1. For NEMA simulation 2, the system sensitivity estimated for a 64 second time period resulted in 4.0 cps/kBq.
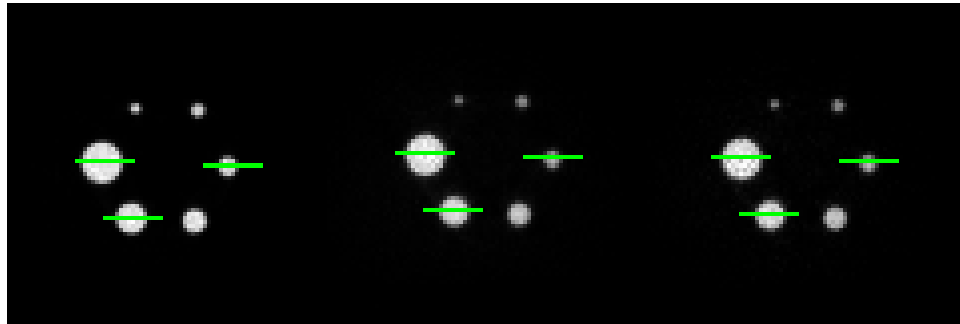
(a) Measurement   (b) NEMA simulation 1   (c) NEMA simulation 2

Figure 9: Profiles over three of the six spheres in the NEMA phantom.

The intensity profiles in figure 9 (a), (b) and (c) are shown in figure 10.
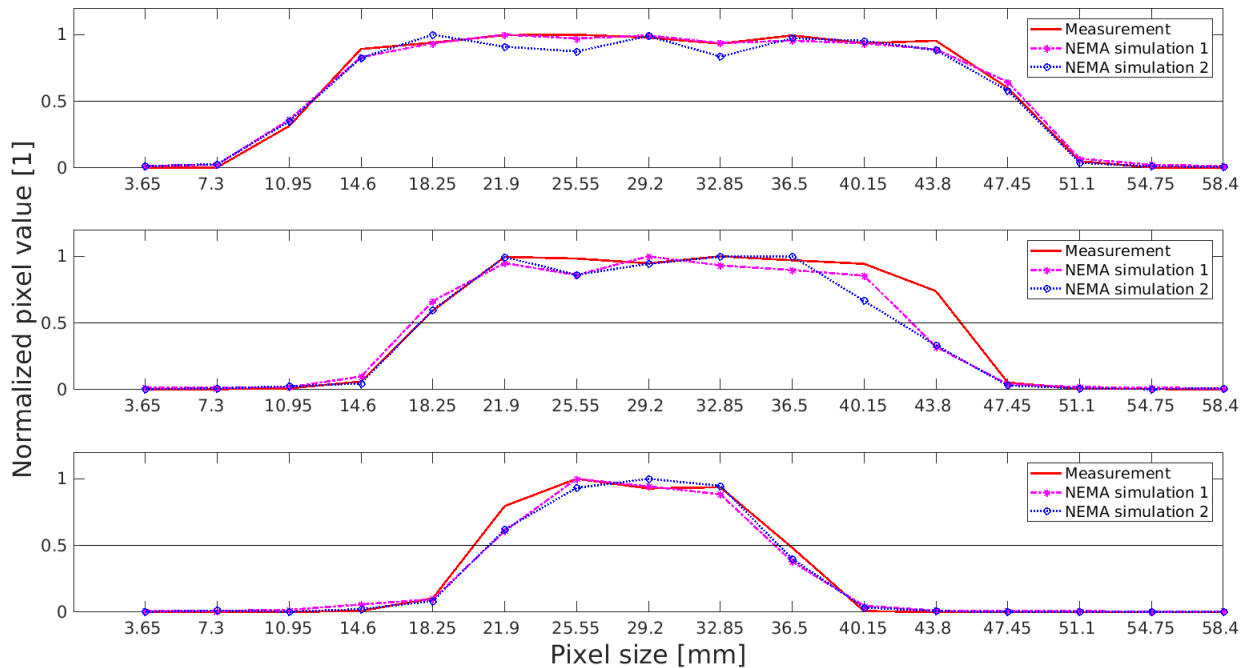
Figure 10: Plot over the spheres in figure 9. The first plot corresponds to the profile of the sphere with the diameter 37 mm, the second plot corresponds to the sphere with the diameter 28 mm and the third plot corresponds to the sphere with the diameter 17 mm.

The FWHM obtained from figure 10, where profiles of three spheres (largest sphere, S_{37}, second largest sphere, S_{28} and the third smallest sphere, S_{17}) are presented in table 4.

Table 4: The FWHM acquired through linear interpolation of the profiles in figure 10.

| | FWHM [mm] | | |
	Measurement	NEMA simulation 1	NEMA simulation 2
S_{37}	36.0	36.4	35.9
S_{28}	27.5	25.4	24.4
S_{17}	16.0	14.5	14.7

5.2 Realistic human-like phantom

Below, in figure 11, are images acquired on a Philips Gemini TF PET/CT of a clinical PET exam with 18F-fluoride.

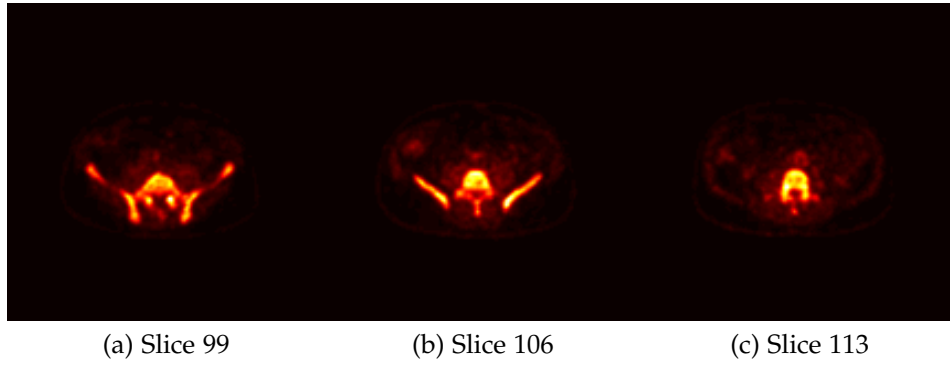(a) Slice 99   (b) Slice 106   (c) Slice 113

Figure 11: Approximately equal slice selection as in figure 12.

The resulting image from the reconstructed data acquired from the XCAT simulation, with the base of the sacrum having an activity concentration of 13 kBq/ml, is shown in figure 12.

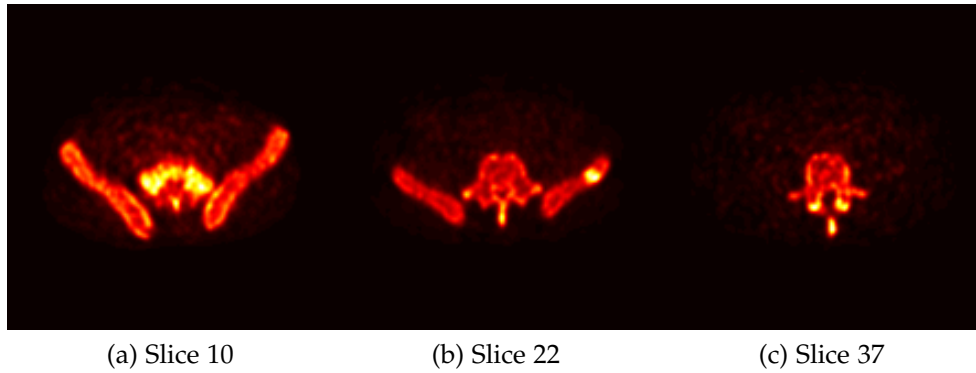(a) Slice 10   (b) Slice 22   (c) Slice 37

Figure 12: CASToR reconstructed simulated data. The different images represent different slices. The middle image contains the randomly distributed tumour.

Images in figure 12 have not been corrected for scattered or random events.

Images in figure 13 are reconstructed data acquired with the SIMIND simulation software. The reconstruction parameters are the same as those used reconstructing the images in figure 12. Images in figure 13 have not been scattered corrected.

Figure 13: SIMIND simulation of the same human-like phantom with activity distribution similar to that of a clinical SPECT exam.

6 Discussion

6.1 Simulations

The world volume (the enclosing logical volume) was set to the relatively small dimensions of {x,y,z} = {1,1,1} m. With relatively small dimensions of the world volume, particles are killed of quicker (as particles exiting the enclosing volume will be terminated), and by doing so, the simulation will effectively be sped up a bit. The scanner used in the simulation was modeled with the G.E. PET/CT Discovery-690 as a template. Certain aspects of the camera were not included such as PMTs and shielding. To a first approximation the modelled scanner was supposed to be generic, so tuning and tweaking the scanners components to exactly replicate the geometry to that of the Discovery-690 would only have taken unnecessary time, and thus, the modelled scanner geometry seemed sufficient enough.

There were two errors that were discovered late into the simulations. One of the errors was that the energy resolution of the LYSO crystals was set to 20%. Reports indicate that that the energy resolution should rather lie in the region of 8% (at 662 keV) [22, 23] (LSO, which shares similar properties have an energy resolution of 10% at 511 keV [3]). The second error that was discovered was a wrongly set energy window width. The energy window threshold was originally set to 300 keV, which also had to be changed. The energy window threshold was adjusted to 425 keV in accordance with the Discovery-690 scanner specifications [19]. As these errors were discovered in a late stage of the thesis there simply was not enough time to re-simulate a complete 120-second simulation of the NEMA phantom. The NEMA simulation 2 was thus only simulated for 64 seconds. That is why there are two different results from the NEMA simulation, the first simulation with the initial parameters (NEMA simulation 1) and the second with the parameters changed (NEMA simulation 2). The XCAT phantom was re-simulated with the changed

25

parameters. These errors occurred due to a mistake, where the initial parameters were accidentally not updated from a test simulation.

The crystals used in the scanner, as mentioned, were LYSO crystals. LYSO consist of several different elements, one of which is Lutetium. A general disadvantage of the LYSO scintillator crystal is that the radioactive isotope ^{176}Lu is naturally occurring, with an abundance of 2.6% [3]. The energy of the subsequently created photons after a ^{176}Lu-decay ranges between 88 - 401 keV [24] and could thus theoretically be a source of noise in a PET acquisition. However, this intrinsic radioactivity has been measured for the G.E. PET/CT Discovery-690, and it was found that the intrinsic rate of true events were approximately 1 cps [25]. Such low rates were considered negligible and were thus not accounted for in the simulation set-up. Dead-time was not accounted for, but there exist models to describe PET systems dead-time characteristics sufficiently, for example, the one proposed by Eriksson et al. [26] could be used.

The NEMA phantom consisted of a matrix with the dimensions of 301x301x83, and in a GATE computational sense will take a very long time to simulate. The fact that 40 MBq was set as the total activity further increased the simulation time. In comparison, the XCAT phantom consisted of a matrix with the dimensions 148x148x41, making the simulation substantially quicker in sense of processing a single event. However, comparisons are hard to make as the total activity of a single simulation constituted of 1.6 MBq. Another factor making it harder to estimate the different computational times depends on how well the nested parametrization fuses nearby voxels (voxels with similar properties are fused together to speed up the simulation). For the XCAT simulation, the reconstructed images constituted of merging ROOT files of the simulation so that the activity concentration in the base of the sacrum became 13.6 kBq/ml (one simulation constituting 2.72 kBq/ml). For the NEMA simulations merging 60 (NEMA simulation 1) and 32 (NEMA simulation 2) ROOT files, each ROOT file simulated for 2 seconds, resulted in a total simulation time of 120 seconds and 64 seconds respectively.

From the first NEMA simulation, a clear deviation with regards to true-, scatter-, and random-fraction can be seen when comparing to that of the measurement. These fractions differ consistently with a factor of about 2. This can partially be explained by the wrongly set energy window and energy resolution. With a low energy resolution, the system will to some degree be unable to distinguish between photons that have undergone scattering from photons that have not. This would explain why there is such an overwhelming amount of scatter and random events in the first NEMA simulation. When the energy resolution and energy window were adjusted for, results approaches those of the measurements. However, the results still have a significant deviation. The mean free path of a 511 keV photon in water is about 7 cm [3], and since the NEMA phantom has a distance from the spheres plane to the inside of the wall of 7 cm (and then some additional thickness of polymethyl methacrylate (PMMA)), one can expect that there will be a substantial amount of scattered and random events, which is seen in table 2. Another thing to note is that the electronic components and scanner shielding were not included in the simulation, components that could potentially add additional

scattered events to the data.

Regarding the total number of coincidences and sensitivity, the first NEMA simulation with a lower energy window is expected to have an increased amount of accepted coincidences compared to the measurement, which can be seen in table 2. Although the second NEMA simulation was not performed for 120 seconds, from the simulated 64 seconds, one can see that the characteristics in the system sensitivity are more comparable. In the first NEMA simulation, one can notice that the system sensitivity deviates with up to 63% from the sensitivity in the measurement. The acquired sensitivities can be compared with reports of 7.5 cps/kBq [25] and with what G.E. themselves specify in their specification sheet of the Discovery-690 camera, with a sensitivity of 7.0 cps/kBq [19]. In the second NEMA simulation, the system sensitivity dropped to 4.0 cps/kBq. A reason as to why the sensitivity now deviates with 22% could potentially be explained by how the density of the LYSO crystal is defined in the GATE material database. In this database, the material LYSO has been assigned the density 5.37 g/cm^3. LYSOs density has been reported to range between 5.37 - 7.1 g/cm^3 [23, 27], and as the attenuation length of a detector depends on the density of the material and the effective atomic number, having a lower density than what is *'true'* would result in a lower γ-ray detection efficiency, and thus a lower system sensitivity.

The curves displaying a normalized intensity profile over three spheres both for the measurement and the NEMA simulations, one can notice similarities between the curves. By measuring the FWHM of the curves this similarity can be confirmed, shown in table 4. Notably is as the object becomes smaller the FWHM starts to deviate a bit. In the visual representation of the measured and simulated image, figure 9, one can notice that the two, and possibly even the three smallest spheres show a decreased contrast. Another thing to note is that the images reconstructed with CASToR were interpolated to fit the dimensions of the images obtained from the measurement. It is possible that the images from the simulation and measurement might not fully coincide due to the interpolation done in CASToR.

Preferably the images from the XCAT simulation would have been compared to images of a clinical 18F-fluoride patient acquired on a Discovery-690. However, there were no patient study images available, images taken on the Discovery-690 could thus not be used. Comparisons were, therefore, instead, done with clinical 18F-fluoride images acquired with a Philips Gemini TF scanner. When comparing the images from the XCAT simulation to the images acquired by the Philips Gemini TF camera, one thing to first point out is that the images from the simulation have been reconstructed using the OSEM method. As the number of iterations increases when reconstructing using MLEM or OSEM the noise will be amplified due to ill-conditioning of the reconstruction problem and because of the intrinsic low count rate inherent in emission tomography [28]. Applying a filter during reconstruction is a proposed solution to handling noise propagation [6], but in that case degradation in spatial resolution may occur. In the worst case scenario, small objects of clinical relevance might even completely disappear. Another solution to reducing the propagation of noise would be to reconstruct using a lesser

number of iterations. The second thing to point out is that the images acquired by the Philips Gemini TF camera have been reconstructed using *BLOB-OS-TF* reconstruction algorithm, a three-dimensional ordered subset time-of-flight reconstruction technique. The inclusion of TOF will reduce noise propagation, by decreasing the uncertainty of where the decay might have occurred along the LOR. For example, the uncertainty in positioning the decay will be within 9 cm for a coincidence timing window of 600 ps. Although this uncertainty is much larger than the typical resolution of PET, which typically is in the orders of a few mm [29, 30], it will reduce the statistical noise by limiting the area to which the noise can propagate. Thus by the inclusion of TOF one can expect a lower presence of noise, or alternatively better signal-to-noise ratio (SNR). The overall structures in the images reconstructed by CASToR from GATE simulations are very similar to the images acquired with the Philips Gemini TF camera - a good indication that the GATE - CASToR chain gives satisfying visual results.

Comparing the GATE and SIMIND simulated images, one first has to state that the SIMIND program is specific to simulating SPECT. The SIMIND simulation was given an activity concentration and distribution similar to that of a clinical exam. Generally, SPECT is expected to have a larger amount of noise present in the image due to the generally lower sensitivity compared to PET. Due to the presence of noise, both images have been filtered during the reconstruction, as all exams would have been. The overall geometrical similarities in reconstructed images, however, seem to coincide very well, another indication that the GATE - CASToR chain gives satisfying results. Changing the modality from SPECT to PET, results in, as one can see comparing figure 12 and 13, better spatial resolution properties. The possibility to simulate using identical phantom with identical source distribution is a good tool if one wants to study and compare the underlying effects between different modalities, such as PET and SPECT.

The results obtained from the NEMA simulation deviates from those of the measurement. This could partially be explained by the modeled scanner not exactly replicating the targeted scanner. The discrepancy in the quantifiable results could (and is expected to) potentially decrease with more time to perfect the simulation set-up, as unnecessary mistakes could be eliminated. The FWHM obtained from the reconstructed CASToR image showed similar properties to those of the measurement, although the smaller spheres seem to have decreased contrast. So, while the pelvic images depict the general structures similar to those taken by the Philips Gemini TF camera it is important to note that the reliability of the results are unknown, as the quantifiable results deviate. Improvements to the model most certainly could be done, to a first approximation the possibility to connect simulated data to reconstructed images are satisfying. Improvements to the model are necessary to further make the quantifiable parameters replicate that of the measurement, as reliable results are essential for the usefulness of a Monte Carlo simulation. Works done by Schmidtlein et al. [31], Zeraatkar et al. [32] and Goinas et al. [33] proves that this most definitely is possible, as their results are in good accordance with their measurements. A suggestion for improvement could be, for example, modelling the system dead-time through the data loss model proposed by Eriksson et al. [26], which could potentially improve the quality of the results. Another correction that

should have been done is the scatter and random correction. CASToR does not provide this feature in the conversion of the ROOT file. Although this is not implemented in the CASToR conversion code the correction could be applied by recovering the scatter and random events for each coupled crystal ID before the conversion, and thus, compute a correction factor for each event manually.

6.2   General thoughts about GATE

This masters thesis consisted largely of learning and understanding how GATE. Learning how to operate GATE can be done through their extensive documentation and the provided benchmark tutorials. Updates are regularly provided to improve the simulation code, and if anything is unclear regardless of GATE-related subject, posting the problem to the GATE mailing-list, a response with a solution will often be provided quickly.

GATEs way of compressing the Geant4 code to fit the purpose of emission tomography means that the user does not have to learn the whole code of Geant4, in the process making it easier to learn and to model modality specific geometries. GATEs design of structuring volumes hierarchically and the neat feature of structural commands allows for a simplistic and logical way to understand how to build and structure the simulation set-up. So while the task is to design complex and comprehensive geometries GATE has made that easy, and through only a few lines of commands, the simulation set-up could be fully described. The main advantage of GATE comes from, as mentioned, the incorporation of the Geant4 kernel as the base for geometry modelling and particle propagation. The possibility of being able to design complex geometries compressed in a small code while still retaining the well-validated physics provided by Geant4 is a huge advantage.

A special feature that GATE offer is the possibility to handle time-dependent phenomena such as respiratory movement. Although Geant4 requires that the simulation geometry is static during particle propagation, this feature of GATE exploits that the duration of an event is much shorter than the time-dependent phenomena in question. The time-dependent phenomena are synchronized with the evolution of the source by dividing the acquisition into several frames, or *'slices'*. For every new frame, the geometry is updated according to supplied commands of predefined motions. This feature of GATE further allows for mimicking highly realistic situations. Another option to mimicking respiratory movement would be to create the XCAT phantom in several time frames - each frame different to the other due to movement. The different time frames could then be simulated in GATE by running multiple acquisitions and then when completed, reconstructed after merging all ROOT files to one file.

While GATE provides highly accurate simulations, that comes at a cost of computational time, and GATE provides a few ways of speeding up the simulation. The use of voxelized phantoms will increase the computational time of GATE significantly, this is due to the general way of how particles are transported by Geant4. Geant4 performs a pre-calculation of volumes so that the time needed to find the next volume/boundary in

29

the geometry during the tracking is reduced. The time needed for this pre-calculation is increased with increasing number of voxels in the phantom. Appropriate algorithms can be used to compress the phantom by fusing adjacent voxels with same materialistic properties, in the process speeding up the simulation by optimising memory and CPU usage [34]. The inclusion of fictitious interaction is another tool that could have been utilised [35]. Appropriate variance reduction techniques (namely splitting and Russian roulette) could have been applied, and particles could have been killed off earlier with the use of larger cuts. However, applying large cuts will ultimately be a trade-off between accuracy and speed since the termination of a particle by a cut will deposit the particles remaining energy locally. Lastly, performing simulations on a GPU or a cluster to speed up the acquisition is an alternative. The simulations were performed on a computer with Intel Xeon E5-1620 processor, with a total of 8 logical cores, this will limit the ability to perform simulations requiring heavy computational power within a reasonable time. The NEMA simulations, for example, were simulated in 2-second periods, each simulation taking approximately 30 hours to complete. To get enough files for a 120-second simulation, performing 8 simulations simultaneously (8 logical cores), this would, if new simulations were started exactly as the previous completed, take 10 days. That for a simulation with a 301x301x83 phantom and with a total activity of 40 MBq. Thus, performing a simulation with a highly detailed voxelized phantom and activity concentration and distribution similar to that of a clinical exam one would *have to* speed up the simulation in order to achieve a reasonable simulating time.

6.3   General thoughts about CASToR

CASToR, the open-source reconstruction software allows users to reconstruct tomographic images from simulated data. CASToR is easy to use with good documentation of the main functions, and if trouble or conundrums arise help from the CASToR community and its developers are often quickly provided. The neat feature of the tool to directly convert a GATE simulation to a CASToR-file makes a great chain from simulated data to reconstructed images. CASToR is designed in a flexible way, allowing users to create their own modules so that missing functions could be implemented to fit the users need.

A neat function of the conversion tool is that it is able to convert several ROOT files into one single CASToR file. That allowed for several simulations to be performed with shorter acquisition time and were instead later added to a single file - by doing so all available logical cores could be taken advantage of.

CASToR will compute the number of events that occurred in the simulation from the ROOT meta-data and then display them. In such a way it is easy to retrieve information regarding the number of prompts, trues, scatters and randoms, in the process making it easy to calculate true-, scatter-, and random-fraction. The scatter and random events are not corrected for in the conversion, and currently, the only way to ignore these events is by using the *-t* option, which will only convert the true coincidences to the CASToR file. By doing so the end result would constitute *'the perfect situation'*, instead a desired

implementation would be to correct for these factors rather than ignoring them during the conversion process. Thus, the images that have been reconstructed using the CASToR software has not been scattered and random corrected, figure 12 and figure 8 (b). Because of this the SIMIND simulated images, shown in figure 13, were chosen not be scatter corrected.

Since the start of this work begun CASToR version 2.0 has been released, including new relevant features, especially the possibility to reconstruct time-of-flight (TOF) data.

6.4   Future prospects

GATE has evolved since its first release in 2004. The release of V6.0 meant major changes to the architecture of the developer layer, and the inclusion of new features making GATE an integrated tool for modelling, dosimetry, and radiotherapy all in the same platform. As of now, V8.0 has been released which includes for example features to use DICOM images as voxelized phantoms, effectively meaning that CT-images in DICOM format could be used directly as a phantom.

Regarding reconstruction, adding a module to perform scatter and random correction to CASToR would be of great interest. Additionally, the inclusion of TOF would be interesting to study but as this thesis started coming to an end there simply was not enough time to further investigate these options.

No estimation of absolute activity was performed, neither in the XCAT simulation nor in the NEMA simulations. This is because the values obtainable from the images reconstructed with CASToR holds no value without a known scaling factor. However, for future work, it would be of great interest to investigate what information the voxel value in CASToR reconstructed images hold.

Ultimately it is the images reconstructed with the manufacturers' scanner algorithms that are evaluated. It would thus be of great interest to be able to reconstruct simulated data with the reconstruction algorithms provided by the manufacturer so that comparisons between simulations and real acquisitions could be performed with the same premise. It would also be interesting if the acquired data could be reconstructed with the CASToR software.

As mentioned earlier, bone scan index is a tool that could be utilised to monitor and evaluate disease progression of bone metastasis using the modality scintigraphy [21]. Future investigations whether GATE could be used as a tool to develop methods on how to quantify 18F-fluoride PET bone scan index would be interesting. In the future possibly serving as an alternative to bone scan indexing with scintigraphy.

Implementing GATE as a tool clinically for development, improvement, and optimisation within the field of medical imaging and therapy would require further investiga-

tions. However, for this to even be a possibility, the simulation time has to be improved so that clinical relevant acquisitions does not take several weeks to perform.

7 Conclusion

GATE is a powerful tool to simulate realistic situations for not only emission tomography, but also applications within transmission tomography and radiation therapy. The Geant4 kernel allows GATE to have the versatility of a general-purpose Monte Carlo program with well-validated physics and comprehensive modelling tools while still being a fairly compressed code, perfect when applications within medical imaging are the desired field of study.

The quantifiable parameters in the NEMA simulation compared to the measurement has a significant deviation, making the true-, scatter-, random-fraction and sensitivity results unreliable. The evaluation with regards to visual properties is satisfying, and the PET images show better spatial resolution over the SPECT images. However, to fully rely on the visual result improvements in the quantifiable parameters have to be done and further be looked upon. Decreasing the time it takes to simulate using GATE to obtain reasonable simulation times is a must. The link between GATE and CASToR provides a good link between simulated data and reconstructed images.

Increasing knowledge of GATE and CASToR would further improve the simulated model, and thus, possibly making GATE simulations an option for patient studies in the future.

8 Acknowledgements

I would like to thank all my supervisors for the support during the thesis.

A special thanks to Michael Ljungberg for all the help during this thesis and for providing material when needed.

Thanks to David Minarik for useful ideas, and for the creation and evolution of this thesis.

Thanks to Cecilia Hindorf for supervising during the preparation and measurement of the NEMA phantom.

9 References

[1] Wang G. Positron Emission Tomography Plays a More Important Role in Health Care. J. Integr. Oncol. 2015 Apr; 4(2):1-2.

[2] Ljungberg M, Strand S-E, King M, editors. Monte Carlo Calculations in Nuclear Medicine. 2nd ed. Boca Raton: CRC Press; 2013

[3] Bailey D, Townsend D, Valk P, Maisey M. Positron Emission Tomography. 1 ed. London: Springer; 2006.

[4] Jadvar H, Praker J.A. Clinical PET and PET/CT. 1 ed. London: Springer; 2005.

[5] Khalil M, editor. Basic Sciences of Nuclear Medicine. 1 ed. Berlin: Springer; 2011.

[6] Tong S, Alessio A, Kinahan P. Image reconstruction for PET/CT scanners: past achievements and future challenges. Imaging med. 2010 Oct;2(5):529-45.

[7] Verdonck P, editor. Advances in Biomedical engineering. Amsterdam: Elsevier; 2009.

[8] James F. A review of pseudorandom number generators. Comput. Phys. Commun. 1990;60(3):329-44.

[9] Lewellen TK, Harrison RL, Vannoy S. The SimSET program, in Monte Carlo calculations. In: Ljungberg M, Strand S, King M, editors. Monte Carlo Calculations in Nuclear Medicine. Philadelphia: Institute of Physics Publishing; 1998.

[10] Ljungberg, M and Strand, SE: A Monte Carlo Program Simulating Scintillation Camera Imaging. Computer Methods and Programs in Biomedicine. 1989;(29):257-72.

[11] Jan S, Santin G, Staelens S, Assié K, Autret D, Avner S, et al. GATE - Geant4 Application for Tomographic Emission: a simulation toolkit for PET and SPECT. Phys Med Biol. 2004;49(19):4543-61.

[12] Agostinelli S, Allison J, Amako K, Apostolakis J, Araujo H, Arce P, et al. Geant4 - a simulation toolkit. Nucl. Instr. Meth. Phys. Res. A. 2003;506(3):250-303.

[13] Von Neumann J. Various Techniques Used in Connection With Random Digits. J. Res. Nat. Bur. Stand. Appl. Math. 1951;3():36-8.

[14] Behrens H, Jänecke J, Schopper H. Numerical Tables for Beta-Decay and Electron Capture. Vol 4. Berlin: Springer; 2006.

[15] Brun R, Rademakers F. ROOT - An Object Oriented Data Analysis Framework. Nucl. Instrum. Methods. Phys. Res. A. 1997;389(2):81-6. See also [`root.cern.ch/`].

[16] Antcheva I, Ballintijn M, Bellenot B, Biskup M, Brun R, Buncic N, et al. ROOT - A C++ framework for petabyte data storage, statistical analysis and visualization. Comput. Phys. Commun. 2009;180(12):2499-2512.

[17] CASToR. Customizable and Advanced Software for Tomographic Reconstruction (CASToR) [Internet]. Available from: `http://www.castor-project.org/sites/default/files/2018-04/CASToR_general_documentation_0.pdf`. See also [`http://www.castor-project.org/`].

[18] PET Phantom - NEMA 2012/IEC 2008 - PET Phantoms - PET Positron Emission Tomography - Nuclear Medicine | Biodex [Internet]. Biodex.com. 2018 [cited 20 May 2018]. Available from: `http://www.biodex.com/nuclear-medicine/products/pet-positron-emission-tomography/pet-phantoms/pet-phantom-nema-2012iec-200`.

[19] GE Healthcare. Discovery PET/CT 690 [pamphlet]. Waukesha: GE Healthcare; 2011.

[20] Segars WP, Sturgeon G, Mendonca S, Grimes J, Tsui BMW. 4D XCAT phantom for multimodality imaging research. Med Phys. 2010;37(9):4902-15.

[21] Nakajima K, Edenbrandt L, Mizokami A. Bone scan index: A new biomarker of bone metastasis in patients with prostate cancer. Int J Urol. 2017;24(9):668-73.

[22] LYSO Scintillation Material [Internet]. Crystals.saint-gobain.com. 2018 [cited 22 May 2018]. Available from: `https://www.crystals.saint-gobain.com/sites/imdf.crystals.com/files/documents/lyso-material-data-sheet.pdf`

[23] Knoll G. Radiation Detection and Measurement. 4th ed. New York: Wiley; 1979.

[24] ENSDF Decay Data in the MIRD Format for 176Lu [Internet]. Nndc.bnl.gov. 2018. [cited 23 May 2018] Available from: `http://www.nndc.bnl.gov/useroutput/176lu_mird.html`

[25] Bettinardi V, Presotto L, Rapisarda E, Picchio M, Gianolli L, Gilardi M C. Physical Performance of the new hybrid PET/CT Discovery-690. Med. Phys. 2011;38(10):5394-5411.

[26] Eriksson L, Wienhard K, Dahlbom M. A Simple Data Loss Model for Positron Camer Systems. IEEE Trans. Nucl. Sci. 1994;41(4):1566-70.

[27] Pepin CM, Berard P, Perrot A-L, Pepin C, Houde D, Lecomte R, et al. Properties of LYSO and recent LSO scintillators for phoswich PET detectors. IEEE Trans. Nucl. Sci. 2004;51(3):789-95.

[28] Shepp LA, Vardi Y. Maximum Likelihood Reconstruction for Emission Tomography. IEEE Trans. Med. Imaging. 1982;1(2):113-22.

[29] Mettler F, Guiberteau M. Essentials of Nuclear Medicine Imaging. 5th ed. Philadelphia: Elsevier Saunders; 2012.

[30] Frey E, Humm J, Ljungberg M. Accuracy and Precision of Radioactivity Quantification in Nuclear Medicine Images. Semin Nucl. Med. 2012;42(3):208-18.

[31] Schmidtlein R, Kirov A, Nehmeh S, Erdi Y, Humm J, Amols H, et al. Validation of GATE Monte Carlo simulations of the GE Advance/Discovery LS PET scanners. Med. Phys. 2006;33(1):198-208.

[32] Zeraatkar N, Ay MR, Kamali-Asl AR, Zaidi H. Accurate Monte Carlo modeling and performance assessment of the X-PET subsystem of the FLEX Triumph preclinical PET/CT scanner. Med Phys. 2011;38():1217-25.

[33] Gonias P, Bertsekas N, Karakatsanis N, Saatsakis G, Gaitanis A, Nikolopoulos D, et al. Validation of a GATE model for the simulation of the Siemens biograph 6 PET scanner. Nucl. Instr. Meth. Phys. Res. A. 2007;571(1-2):263-6.

[34] Taschereau R, Chatziioannou A. Compressed Voxels for High-Resolution Phantom Simulations in GATE. Phys. Med. Biol. 2008;10(1):40-7.

[35] Rehfeld N, Stute S, Apostolakis J, Soret M, Buvat I. Introducing improved voxel navigation and fictitous interaction tracking in GATE for enhanced efficiency. Phys. Med. Biol. 2009;54(7):2163-78.